GEOLOGY | THE GEOLOGICAL SOCIETY OF AMERICA®

https://doi.org/10.1130/G54232.1

Manuscript received 24 November 2025
Revised manuscript received 18 December 2025
Manuscript accepted 4 January 2026

Published online 22 January 2026

From wide rifts to orogens: A new perspective for Proterozoic tectonics

Youseph Ibrahim[1,*] and Patrice F. Rey[2]
[1]Earth and Environmental Science, James Cook University, Townsville, Queensland 4811, Australia
[2]School of Geosciences, University of Sydney, Sydney, New South Wales 2006, Australia

ABSTRACT

The thermal structure of the lithosphere influences both the extensional and contractional phases of rift-inversion orogenesis. During the Proterozoic, elevated geotherms likely favored wide rift formation, yet examples of wide rift-inversion orogens are absent from the literature. Using 2-D thermo-mechanical models, we show that narrow rifts formed under colder initial geotherms invert into localized orogenic wedges flanked by foreland basins, largely utilizing rift architecture. Wide rifts formed under warmer initial geotherms, representing Proterozoic conditions, invert into broad, low-relief orogenic plateaus through distributed upper crustal faulting and ductile flow in the underlying lithosphere. Importantly, postrift tectonic quiescence modestly affects narrow rift inversion, primarily widening the orogenic wedge, but fundamentally alters wide rift inversion by promoting lithospheric cooling, embrittlement, and the development of deep contractional shear zones offsetting the Moho by 10–20 km. This wide rift-inversion framework may provide an explanation for distributed shortening and low topographic relief in Proterozoic orogens.

INTRODUCTION

The thermal state of the lithosphere governs the first-order structural evolution of both orogens and rifts. During orogenesis, cold, strong lithosphere localizes strain into narrow, elevated orogenic wedges surrounded by flexural basins, whereas hot, weak lithosphere distributes deformation across broad, low-elevation orogenic plateaus (Rey and Houseman, 2006; Beaumont et al., 2006). Similarly, under extension, cooler conditions produce localized, narrow rifts flanked by flexural rift-shoulder uplifts, while higher temperatures promote widespread deformation, resulting in wide rifts (Buck, 1991; Brun, 1999). In the Archean and Proterozoic, hotter average geotherms relative to modern conditions likely made broad orogenic plateaus and wide rifts the dominant mode of continental contraction and extension, respectively (Brown, 2007; Rey and Coltice, 2008; Spencer et al., 2021). Yet, examples of Proterozoic to Archean wide rifts and inverted wide rifts are virtually nonexistent in the literature, possibly because they have not been recognized as such. Consequently, these ancient terrains are commonly interpreted through modern geodynamic frameworks, an approach that becomes less applicable deeper in geological time. To investigate extensional and contractional deformation in deep time, we use 2-D thermo-mechanical experiments to examine rift-inversion orogen evolution under contrasting initial thermal regimes representative of Phanerozoic and Paleoproterozoic to Mesoproterozoic conditions. We place particular emphasis on the postrift phase of tectonic quiescence, during which lithospheric cooling and strengthening occur (Doré et al., 1999; Naliboff and Buiter, 2015).

We show that regardless of the duration of postrift quiescence, inverted narrow rifts utilize pre-existing rift architecture to form an elevated orogenic wedge flanked by flexural basins. By contrast, the mode of wide rift inversion depends on the duration of postrift tectonic quiescence. When it is short or nil, inverted wide rifts form broad, low-elevation plateaus without flexural basins. When postrift quiescence lasts for several tens of millions of years, lithospheric cooling and embrittlement lead to coupling between short-lived upper crustal faults and long-lived upper mantle shear zones, producing significant Moho offset beneath the broad, low-elevation plateau. We compare the patterns derived from our numerical experiments to natural analogs that may be interpreted through this wide rift-inversion framework.

NUMERICAL METHODS AND MODEL SETUP

We present two suites of 2-D thermo-mechanical experiments comparing narrow and wide rift inversion. Numerical experiments employ Underworld 2, an open-source finite-element geodynamic framework (Moresi et al., 2007), to solve Stokes flow (governing equations in Text S1 in the Supplemental Material[1]) on a 680 × 220 km lithosphere-asthenosphere domain (Fig. 1) discretized on a Cartesian, nondeforming grid with 500 m resolution (1360 × 440 elements). Narrow rift and wide rift scenarios are distinguished by geotherms yielding Moho temperatures of 600 °C (MT600 experiment) and 800 °C (MT800 experiment), respectively. The lithosphere-asthenosphere boundary is defined by the 1300 °C isotherm.

Materials have a viscoplastic rheology with temperature-, strain-, stress rate–, stress-, and melt-dependent viscosity (Tables S2–S3 in the Supplemental Material). Plastic behavior follows a Drucker-Prager yield criterion with strain weakening that linearly reduces cohesion (10×) and friction coefficient (5× in the crust, 10× in the mantle) as accumulated plastic strain evolved from 0% to 15%. Partial melting reduces density by 13% and viscosity by up to 1000× (crust) and 100× (mantle). Melt fractions are capped

Youseph Ibrahim https://orcid.org/0000-0003-4803-5141
*youseph.ibrahim@jcu.edu.au

[1]Supplemental Material. Governing equations and additional information on numerical experiments, additional experiment figures, and links to experiment scripts. Please visit https://doi.org/10.1130/GEOL.S.31051504 to access the supplemental material; contact editing@geosociety.org with any questions.

CITATION: Ibrahim, Y., and Rey, P.F., 2026, From wide rifts to orogens: A new perspective for Proterozoic tectonics: Geology, v. XX, p. , https://doi.org/10.1130/G54232.1

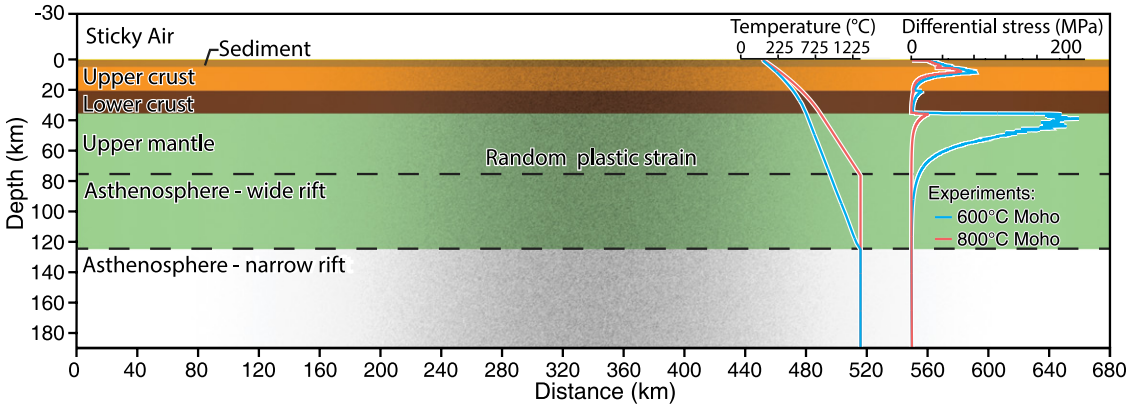

Figure 1. Initial state of numerical experiments showing material distribution, seeded accumulated plastic strain following Gaussian distribution (black shading), temperature profiles, and deviatoric stress profiles under extensional boundary conditions at experiment start.

at 30% (crust) and 2% (mantle), given that melt segregation is not modeled. Solidus and liquidus parameters are detailed in Text S1. Sedimentation and erosion occur at 1 mm yr^{-1} below and above sea level, respectively. Horizontal free slip is permitted at the model top and base. A kinematic isostasy condition maintains constant basal pressure by allowing the asthenosphere to flow in and out of the model base. To mitigate boundary effects, we introduce random plastic strain noise that follows a centered Gaussian distribution with a maximum plastic strain of 15% (Fig. 1).

Each experiment undergoes 25% extension over 8 m.y., followed by 25% contraction over 8 m.y., using horizontal velocities (V_x) of ±2.146 cm yr^{-1} at the left and right walls, delivering an average strain rate of 10^{-15} s^{-1}. For both the narrow and wide rifts, we test inversion after 0, 20, 40, and 60 m.y. of tectonic quiescence (i.e., V_x is nil) during which thermal relaxation, sedimentation, and erosion proceed.

RESULTS

Rift Phase

Extension of the MT600 experiment produces a narrow rift initiating with conjugate normal faults in the upper crust. This forms a pair of grabens that widen as faults evolve into listric detachments merging at the brittle-ductile transition. The lower crust thins progressively and homogeneously, while mantle faults rotate to subhorizontal as the exhuming asthenosphere undergoes decompression melting. After 8 m.y. of extension, the basin reaches ~300 km width with ≤7 km of synrift sediment deposited over crust thinned to <10% of its original thickness (Fig. 2A).

Extension of the MT800 experiment produces a wide rift accommodated by broadly distributed, synchronous normal faults in the upper crust. A thin (<3 km) synrift sediment layer is uniformly deposited across the model. The ductile lower crust and lithospheric mantle are extended and thinned homogeneously, while the Moho remains flat. Gentle and broad asthenospheric exhumation occurs, with decompression partial melting restricted to the lower crust only (Fig. 2B).

Inversion Phase

Inversion of the narrow rift immediately after cessation of extension leads to basin uplift accommodated by reactivation of the basin-bounding listric normal faults, generating up to 3.8 km of topography (Fig. 3A). Flexural foreland basins develop on the flanks of the elevated region due to isostatic adjustment in response to the orogenic load and underthrusting of extended, weakened lithospheric margins beneath the detached rift basin. With continued shortening, deformation propagates outward into the foreland. In the lower crust, convergence is accommodated by a combination of ductile folding and shearing, and in the mantle, by viscous flow within the asthenospheric dome separating the rifted lithospheric margins and by

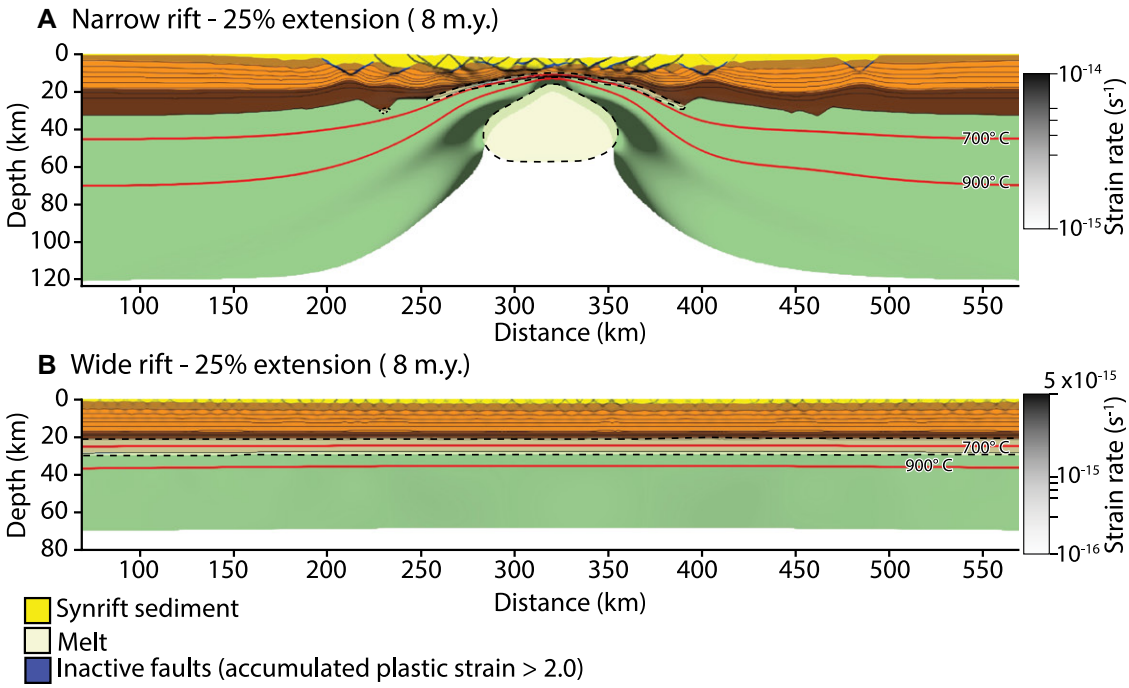

Figure 2. Experiments after 8 m.y. of rifting under thermal conditions favoring narrow rift (MT600) (A) and wide rift (MT800) (B) modes of continental extension. Accumulated plastic strain is mapped on inactive faults, while strain rate marks active faults. Dashed line outlines partial melting. Views are cropped to emphasize deforming regions.

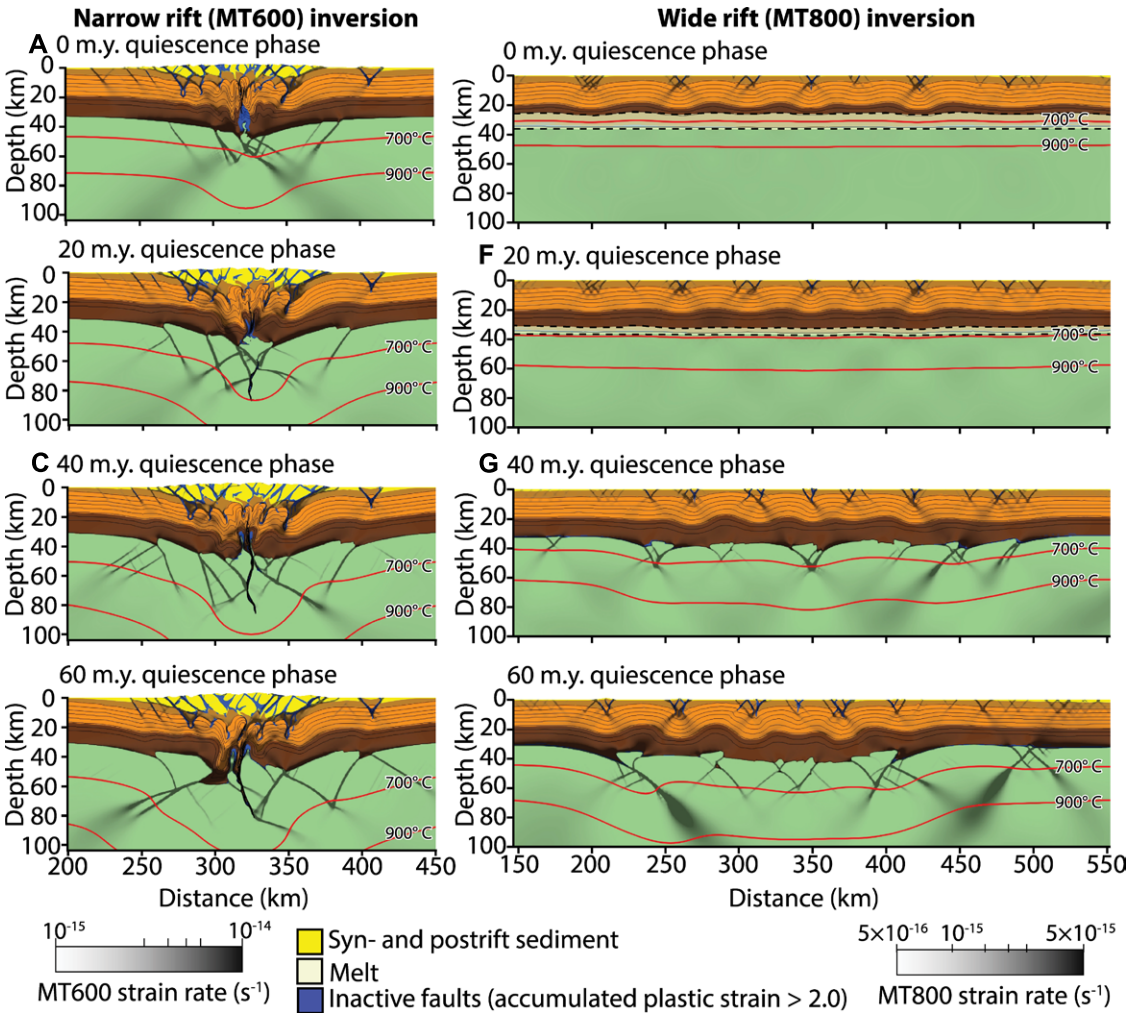

Figure 3. (A–D) Narrow rift (MT600) inversion after 0 m.y. (A), 20 m.y. (B), 40 m.y. (C), and 60 m.y. (D) of quiescence. (E–H) Wide rift (MT800) inversion after 0 m.y. (E), 20 m.y. (F), 40 m.y. (G), and 60 m.y. (H) of quiescence. Views are cropped to emphasize deforming regions.

newly formed reverse faults in the lithospheric mantle. Longer postrift quiescence and thermal sagging periods enable thicker sediment accumulation, producing wider, higher orogens with more prominent flexural basins upon inversion (Figs. 3B–3D).

Inversion of the wide rift immediately after cessation of extension produces a broad, low-elevation plateau, primarily accommodated by reactivation of pre-existing normal faults and homogenous thickening and ductile buckling in the lower crust and lithospheric mantle (Fig. 3E). Broad antiforms and narrow synforms develop in the lower crust beneath active upper crustal faults, while the Moho remains relatively flat. The duration of postrift tectonic quiescence strongly impacts wide rift inversion architecture. Inversion after 20 m.y. postrift quiescence leads to a diffuse low-strain zone around the Moho (Fig. 3F). Following ≥40 m.y. quiescence, significant lithospheric mantle cooling and embrittlement shift the deformation style from distributed ductile deformation to localized shear zones, while crustal deformation remains relatively distributed and focused on the inversion of pre-existing normal faults (Figs. 3G and 3H). Inversion after 60 m.y. quiescence accentuates the contrast in contractional styles between the crust and mantle. In the upper crust, thrust faults are distributed across the model length, whereas the lower crust buckles. Beneath the crust, some pronounced shear zones crosscut the lithospheric mantle, forcing the underthrusting of some segments of lithospheric mantle (Fig. 3H). Despite significant convergence, surface uplift is minimal because prolonged cooling increases lithospheric mantle thickness more than thermal sagging and sedimentation increases crustal thickness. The resulting post-contractional architecture includes pronounced Moho offsets and a lithospheric mantle affected by ductile shear zones controlling the formation of pop-ups and pop-downs, as well as mantle underthrusting at the limits of the orogenic domain (Fig. 3H).

DISCUSSION AND FIELD EXAMPLES

Although a period of postrift tectonic quiescence does not substantially affect inversion outcomes of narrow rifts, a long (>40 m.y.) period of postrift tectonic quiescence and cooling considerably impacts the inversion of wide rifts. Prolonged cooling alters the mechanical stratification of wide rift lithosphere, which, upon inversion, enables the development of prominent mantle shear zones that offset the Moho. In the upper crust, inversion leads to distributed shortening through the development of a broad fold-and-thrust belt (Fig. 3H). Importantly, lithospheric cooling leads to the strengthening of the mantle, whereas the continental crust, weakened by the formation of a broad array of normal faults, remains comparatively weak. This explains the distributed and localized nature of deformation in the crust and the mantle, respectively.

Our experiments agree with those of Vasey et al. (2024), who found that wide rift inversion results in distributed thickening and that postrift cooling enhances deformation localization. Our experiments indicate that this localization is most pronounced in the lithospheric mantle, while crustal deformation remains broadly distributed. This pattern is also supported by analog experiments (Samsu et al., 2023), which demonstrate that increased mantle strength promotes strain localization via folding in the lower crust, in contrast to a weaker mantle, which favors homogeneous thickening.

The deformation patterns identified in our wide rift inversion experiments provide a pre-

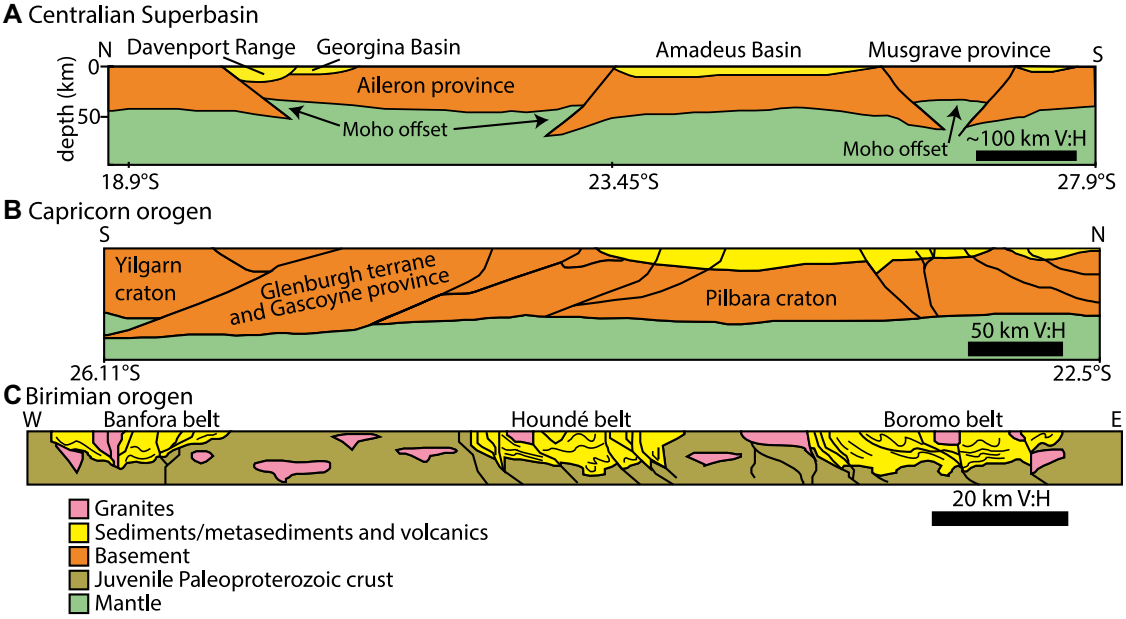

Figure 4. (A) Schematic crustal structure across central Australia. Modified from Sippl (2016). (B) Cross section across Capricorn orogen. Modified from Johnson et al. (2013). (C) Schematic cross section across western Burkina Faso within the Birimian orogen. Modified from Baratoux et al. (2011).

dictive framework, particularly relevant to the Paleoproterozoic to Mesoproterozoic. Our models consistently produce characteristic features, such as broad, low-relief plateaus, and distributed upper crustal shortening. These features are consistent with mid-Proterozoic orogens marked by high-temperature metamorphism, limited crustal thickening, and low surface relief (Spencer et al., 2021). In addition, our experiments reveal deep Moho-offsetting mantle shear zones in thermally relaxed wide rifts. Together, these features offer criteria for recognizing wide rift inversion in the geological record. In what follows, we examine orogens that may exhibit some of these characteristics within a framework of wide rift inversion.

Drawing comparisons between numerical experiments and ancient orogens, eroded and re-equilibrated both thermally and mechanically, is inherently speculative. Our field examples highlight that Proterozoic regions with broad contractional deformation may represent inverted wide rifts, providing a new interpretive framework for future investigation.

Centralian Superbasin: Wide Rift Inversion Following Protracted Tectonic Quiescence

The Centralian Superbasin of Australia is a broadly distributed Proterozoic basin (Walter et al., 1995) that initiated with widespread rifting between ca. 1085 and 1040 Ma under hot lithospheric conditions (Aitken et al., 2013; Alghamdi et al., 2018). Rifting was followed by prolonged quiescence and thermal recovery (Korsch and Lindsay, 1989; Glorie et al., 2017) until 570 Ma. Up to 7 km, and locally as much as 12 km, of Neoproterozoic sediments was deposited across several subbasins (Haines et al., 2016). Given that thermal sagging rarely exceeds 2–3 km (Middleton, 1989), it is possible that the deposition of Neoproterozoic sediments occurred during wide rifting at low strain rates accompanied by thermal recovery and sagging (Lindsay et al., 1987; Camacho et al., 2015; Smithies et al., 2015). The Centralian Superbasin was inverted during the Petermann orogeny (570–530 Ma) and the Alice Springs orogeny (450–300 Ma). Broad upper crustal deformation and reactivation migrated from the southern portions of the Centralian Superbasin during the Petermann orogeny to the northern portions during the Alice Springs orogeny (Hand and Sandiford, 1999; Gibson and Edwards, 2020). Consistent with our experiments (Fig. 3H), these inversion events are associated with shear zones (e.g., the Redbank shear zone) that offset the Moho by up to 20–25 km (Aitken et al., 2009; Sippl, 2016; Fig. 4A). These Moho-offsetting shear zones may result from shortening after postrift tectonic quiescence and cooling.

Capricorn Orogen: Wide Rift Inversion and Limited Tectonic Quiescence

The Capricorn orogen may serve as an analog for the inversion of early Proterozoic wide rifts under hot lithospheric conditions. In the western Australian craton, late Archean to Early Proterozoic distributed intracratonic rifts (Krapez and Martin, 1999) were repeatedly reactivated through a series of contractional events associated with progressive suturing of the Yilgarn and Pilbara cratons, including the Ophthalmian (ca. 2200 Ma), Glenburgh (2000–1960 Ma), and Capricorn (1830–1780 Ma) orogenies (Johnson et al., 2013, and references therein). Protracted medium- to high-grade metamorphism and crustal melting indicate sustained warm conditions during shortening (Cawood and Tyler, 2004). Crustal-scale seismic data reveal distributed deformation across the orogen and several major lithospheric faults (Fig. 4B; Johnson et al., 2013). Such features are compatible with the inversion of a wide rift.

Birimian Orogen

The Paleoproterozoic Birimian orogen of the West African craton may tentatively be interpreted as a wide rift formed in juvenile oceanic crust that later underwent multiple phases of inversion (Baratoux et al., 2011). Features consistent with wide rifting include shallow volcano-sedimentary subbasins distributed over >1000 km (Grenholm, 2019). The postinversion architecture is the result of broadly distributed contractional deformation accommodated by steep faults and transpressional shear zones, producing limited topographic relief (Fig. 4C; Baratoux et al., 2011). These features are consistent with the inversion of a hot, mechanically weak wide rift, resulting in a broad, low-elevation orogenic plateau.

CONCLUSIONS

Wide rifting and wide rift-inversion orogenesis may have been dominant modes of continental extension and contraction from the Paleoproterozoic to Mesoproterozoic, producing orogenic architectures that differ from those generated by narrow rift inversion. Inverted narrow rifts form elevated orogenic wedges through reactivation of basin-bounding faults flanked by foreland basins. Conversely, wide rift inversion produces broad low-elevation plateaus through reactivation of upper crustal faults and ductile flow in the lower crust. Postrift tectonic quiescence does not significantly impact narrow rift inversion beyond widening the orogenic wedge. The style of wide rift-inversion orogens, however, is sensitive to the duration of postrift tectonic quiescence. Cooling during tectonic quies-

cence leads to lithospheric embrittlement, which facilitates the formation of deep lithospheric shear zones that offset the Moho by 10–20 km beneath a broad low-elevation plateau. These results highlight postrift cooling as a first-order control on the inversion styles of wide rifts, a regime likely prevalent under Proterozoic thermal conditions, and suggest that the concept of wide rift-inversion orogens offers a new framework to understand contractional tectonics in the Proterozoic.

ACKNOWLEDGMENTS

We thank our reviewers for their constructive feedback. This work was funded by Australian Research Council grants ARC-LP190100146 and ARC-DP220100709, with computing support from the Australian National Computational Infrastructure and Underworld provided by AuScope.

REFERENCES CITED

Aitken, A.R.A., Betts, P.G., Weinberg, R.F., and Gray, D., 2009, Constrained potential field modeling of the crustal architecture of the Musgrave Province in central Australia: Evidence for lithospheric strengthening due to crust-mantle boundary uplift: Journal of Geophysical Research, v. 114, B12405, https://doi.org/10.1029/2008JB006194.

Aitken, A.R.A., Smithies, R.H., Dentith, M.C., Joly, A., Evans, S., and Howard, H.M., 2013, Magmatism-dominated intracontinental rifting in the Mesoproterozoic: The Ngaanyatjarra Rift, central Australia: Gondwana Research, v. 24, p. 886–901, https://doi.org/10.1016/j.gr.2012.10.003.

Alghamdi, A.H., Aitken, A.R.A., and Dentith, M.C., 2018, The deep crustal structure of the Warakurna LIP, and insights on Proterozoic LIP processes and mineralisation: Gondwana Research, v. 56, p. 1–11, https://doi.org/10.1016/j.gr.2017.12.001.

Baratoux, L., Metelka, V., Naba, S., Jessell, M.W., Grégoire, M., and Ganne, J., 2011, Juvenile Paleoproterozoic crust evolution during the Eburnean orogeny (~2.2–2.0 Ga), western Burkina Faso: Precambrian Research, v. 191, p. 18–45, https://doi.org/10.1016/j.precamres.2011.08.010.

Beaumont, C., Nguyen, M.H., Jamieson, R.A., and Ellis, S., 2006, Crustal flow modes in large hot orogens, *in* Law, R.D., Searle, M.P., and Godin, L., eds., Channel Flow, Ductile Extrusion and Exhumation in Continental Collision Zones: Geological Society, London, Special Publication 268, p. 91–145, https://doi.org/10.1144/GSL.SP.2006.268.01.05.

Brown, M., 2007, Metamorphic conditions in orogenic belts: A record of secular change: International Geology Review, v. 49, p. 193–234, https://doi.org/10.2747/0020-6814.49.3.193.

Brun, J.-P., 1999, Narrow rifts versus wide rifts: Inferences for the mechanics of rifting from laboratory experiments: Philosophical Transactions of the Royal Society of London, Series A: Mathematical, Physical and Engineering Sciences, v. 357, p. 695–712, https://doi.org/10.1098/rsta.1999.0349.

Buck, W.R., 1991, Modes of continental lithospheric extension: Journal of Geophysical Research, v. 96, p. 20,161–20,178, https://doi.org/10.1029/91JB01485.

Camacho, A., Armstrong, R., Davis, D.W., and Bekker, A., 2015, Early history of the Amadeus Basin: Implications for the existence and geometry of the Centralian Superbasin: Precambrian Research, v. 259, p. 232–242, https://doi.org/10.1016/j.precamres.2014.12.004.

Cawood, P.A., and Tyler, I.M., 2004, Assembling and reactivating the Proterozoic Capricorn Orogen: Lithotectonic elements, orogenies, and significance: Precambrian Research, v. 128, p. 201–218, https://doi.org/10.1016/j.precamres.2003.09.001.

Doré, A.G., Lundin, E.R., Jensen, L.N., Birkeland, Ø., Eliassen, P.E., and Fichler, C., 1999, Principal tectonic events in the evolution of the northwest European Atlantic margin, *in* Fleet, A.J., and Boldy, S.A.R., eds., Petroleum Geology of Northwest Europe: Proceedings of the 5th Conference: Geological Society, London, Petroleum Geology Conference Series 5, p. 41–61, https://doi.org/10.1144/0050041.

Gibson, G.M., and Edwards, S., 2020, Basin inversion and structural architecture as constraints on fluid flow and Pb–Zn mineralization in the Paleo–Mesoproterozoic sedimentary sequences of northern Australia: Solid Earth, v. 11, p. 1205–1226, https://doi.org/10.5194/se-11-1205-2020.

Glorie, S., Agostino, K., Dutch, R., Pawley, M., Hall, J., Danišík, M., Evans, N.J., and Collins, A.S., 2017, Thermal history and differential exhumation across the Eastern Musgrave Province, South Australia: Insights from low-temperature thermochronology: Tectonophysics, v. 703–704, p. 23–41, https://doi.org/10.1016/j.tecto.2017.03.003.

Grenholm, M., 2019, The global tectonic context of the ca. 2.27–1.96 Ga Birimian Orogen—Insights from comparative studies, with implications for supercontinent cycles: Earth-Science Reviews, v. 193, p. 260–298, https://doi.org/10.1016/j.earscirev.2019.04.017.

Haines, P.W., Kirkland, C.L., Wingate, M.T.D., Allen, H., Belousova, E.A., and Gréau, Y., 2016, Tracking sediment dispersal during orogenesis: A zircon age and Hf isotope study from the western Amadeus Basin, Australia: Gondwana Research, v. 37, p. 324–347, https://doi.org/10.1016/j.gr.2015.08.011.

Hand, M., and Sandiford, M., 1999, Intraplate deformation in central Australia, the link between subsidence and fault reactivation: Tectonophysics, v. 305, p. 121–140, https://doi.org/10.1016/S0040-1951(99)00009-8.

Johnson, S.P., et al., 2013, Crustal architecture of the Capricorn Orogen, Western Australia and associated metallogeny: Australian Journal of Earth Sciences, v. 60, p. 681–705, https://doi.org/10.1080/08120099.2013.826735.

Korsch, R.J., and Lindsay, J.F., 1989, Relationships between deformation and basin evolution in the intracratonic Amadeus Basin, central Australia: Tectonophysics, v. 158, p. 5–22, https://doi.org/10.1016/0040-1951(89)90312-0.

Krapez, B., and Martin, D.M., 1999, Sequence stratigraphy of the Palaeoproterozoic Nabberu Province of Western Australia: Australian Journal of Earth Sciences, v. 46, p. 89–103, https://doi.org/10.1046/j.1440-0952.1999.00692.x.

Lindsay, J.F., Korsch, R.J., and Wilford, J.R., 1987, Timing the breakup of a Proterozoic supercontinent: Evidence from Australian intracratonic basins: Geology, v. 15, p. 1061–1064, https://doi.org/10.1130/0091-7613(1987)15<1061:TTBOAP>2.0.CO;2.

Middleton, M.F., 1989, A model for the formation of intracratonic sag basins: Geophysical Journal International, v. 99, p. 665–676, https://doi.org/10.1111/j.1365-246X.1989.tb02049.x.

Moresi, L., Quenette, S., Lemiale, V., Mériaux, C., Appelbe, B., and Mühlhaus, H.-B., 2007, Computational approaches to studying nonlinear dynamics of the crust and mantle: Physics of the Earth and Planetary Interiors, v. 163, p. 69–82, https://doi.org/10.1016/j.pepi.2007.06.009.

Naliboff, J., and Buiter, S.J.H., 2015, Rift reactivation and migration during multiphase extension: Earth and Planetary Science Letters, v. 421, p. 58–67, https://doi.org/10.1016/j.epsl.2015.03.050.

Rey, P.F., and Coltice, N., 2008, Neoarchean lithospheric strengthening and the coupling of Earth's geochemical reservoirs: Geology, v. 36, p. 635–638, https://doi.org/10.1130/G25031A.1;.

Rey, P.F., and Houseman, G., 2006, Lithospheric scale gravitational flow: The impact of body forces on orogenic processes from Archaean to Phanerozoic, *in* Buiter, S.J.H., and Schreurs, G., eds., Analogue and Numerical Modelling of Crustal-Scale Processes: Geological Society, London, Special Publication 253, p. 153–167, https://doi.org/10.1144/GSL.SP.2006.253.01.08.

Samsu, A., Gorczyk, W., Schmid, T.C., Betts, P.G., Cruden, A.R., Morton, E., and Amirpoorsaeed, F., 2023, Selective inversion of rift basins in lithospheric-scale analogue experiments: Solid Earth, v. 14, p. 909–936, https://doi.org/10.5194/se-14-909-2023.

Sippl, C., 2016, Moho geometry along a north–south passive seismic transect through Central Australia: Tectonophysics, v. 676, p. 56–69, https://doi.org/10.1016/j.tecto.2016.03.031.

Smithies, R.H., Kirkland, C.L., Korhonen, F.J., Aitken, A.R.A., Howard, H.M., Maier, W.D., Wingate, M.T.D., Quentin de Gromard, R., and Gessner, K., 2015, The Mesoproterozoic thermal evolution of the Musgrave Province in central Australia—Plume vs. the geological record: Gondwana Research, v. 27, p. 1419–1429, https://doi.org/10.1016/j.gr.2013.12.014.

Spencer, C.J., Mitchell, R.N., and Brown, M., 2021, Enigmatic mid-Proterozoic orogens: Hot, thin, and low: Geophysical Research Letters, v. 48, https://doi.org/10.1029/2021GL093312.

Vasey, D.A., Naliboff, J.B., Cowgill, E., Brune, S., Glerum, A., and Zwaan, F., 2024, Impact of rift history on the structural style of intracontinental rift-inversion orogens: Geology, v. 52, p. 429–434, https://doi.org/10.1130/G51489.1.

Walter, M.R., Veevers, J.J., Calver, C.R., and Grey, K., 1995, Neoproterozoic stratigraphy of the Centralian Superbasin, Australia: Precambrian Research, v. 73, p. 173–195, https://doi.org/10.1016/0301-9268(94)00077-5.

Printed in the USA